

NATF (Native and Tissue-Specific Fluorescence): A Strategy for Bright, Tissue-Specific GFP Labeling of Native Proteins in *Caenorhabditis elegans*

Siwei He,^{*,†} Andrea Cuentas-Condori,[†] and David M. Miller, III^{*,†,1}

^{*}Program in Neuroscience, Vanderbilt University, Nashville, Tennessee and [†]Department of Cell and Developmental Biology, Vanderbilt University School of Medicine, Nashville, Tennessee 37240

ORCID IDs: 0000-0002-4847-0031 (A.C.-C.); 0000-0001-9048-873X (D.M.M.)

ABSTRACT GFP labeling by genome editing can reveal the authentic location of a native protein, but is frequently hampered by weak GFP signals and broad expression across a range of tissues that may obscure cell-specific localization. To overcome these problems, we engineered a Native And Tissue-specific Fluorescence (NATF) strategy that combines genome editing and split-GFP to yield bright, cell-specific protein labeling. We use clustered regularly interspaced short palindromic repeats CRISPR/Cas9 to insert a tandem array of seven copies of the GFP11 β -strand (*gfp11_{x7}*) at the genomic locus of each target protein. The resultant *gfp11_{x7}* knock-in strain is then crossed with separate reporter lines that express the complementing split-GFP fragment (*gfp1-10*) in specific cell types, thus affording tissue-specific labeling of the target protein at its native level. We show that NATF reveals the otherwise undetectable intracellular location of the immunoglobulin protein *OIG-1* and demarcates the receptor auxiliary protein *LEV-10* at cell-specific synaptic domains in the *Caenorhabditis elegans* nervous system.

KEYWORDS *C. elegans*; cell specificity; genome editing; GFP; NATF; native expression; protein localization

RELIABLE localization of a given protein can provide useful clues to its mechanism of action. One way to achieve this goal is to label the protein of interest with tags, such as fluorescent proteins (e.g., GFP) (Chalfie 2009; Remington 2011) or small peptides (e.g., FLAG or HA) (Terpe 2003). Because tagged proteins are typically expressed with heterologous promoters or from multicopy transgenic arrays, this approach can result in misleading signals due to overexpression (Praitis *et al.* 2001). This problem can be obviated by using clustered regularly interspaced short palindromic repeats (CRISPR)/Cas9 for single-copy labeling of the native protein (Hsu *et al.* 2014; Dickinson *et al.* 2015), but this genome-editing strategy suffers from two additional limitations. First, the endogenous expression level of a target protein may be too low for detection. Second, the protein of

interest may be expressed in several tissues, thus preventing a clear delineation of cell-specific localization. Previous efforts have focused on solving each of these problems separately. For example, strategies to enhance detection include the use of brighter fluorescent proteins (El Mouridi *et al.* 2017; Hostettler *et al.* 2017) and the development of the SunTag label, which uses a scaffold-like structure to recruit multiple copies of GFP (Tanenbaum *et al.* 2014). The “FLP-on” strategy uses cell-specific FLP drivers to activate GFP expression from CRISPR/Cas9-engineered FRT sites but may not yield a visible signal for low-expressing genes (Schwartz and Jorgensen 2016). Here, we describe an experimental approach, NATF (Native And Tissue-specific Fluorescence or “Native”), that exploits a combinatorial strategy to achieve both bright and cell-specific labeling of the protein of interest.

Our approach relies on the finding that the barrel-like GFP structure can be reconstituted by the spontaneous interaction of two separate GFP peptides derived from the highly stable GFP variant, superfolder GFP. The larger of these fragments is comprised of the first 10 β -strands (GFP1-10). Its smaller complement, a short, 16 amino acid sequence, contains the 11th β -strand (GFP11) (Cabantous *et al.* 2005). The reconstituted

Copyright © 2019 by the Genetics Society of America
doi: <https://doi.org/10.1534/genetics.119.302063>

Manuscript received February 27, 2019; accepted for publication March 28, 2019; published Early Online April 5, 2019.

Available freely online through the author-supported open access option.

Supplemental material available at <https://doi.org/10.25386/genetics.7898075>.

¹Corresponding author: Department of Cell and Developmental Biology, Vanderbilt University Medical Center, Vanderbilt University School of Medicine, 3120 MRBIII, Nashville, TN 37232-8240. E-mail: david.miller@vanderbilt.edu

split-GFP hybrid produces a fluorescent signal that is substantially brighter than weak background fluorescence arising from overexpression of the GFP1-10 fragment (Feng *et al.* 2017). Thus, to enhance the GFP signal, a target protein can be tagged with multiple copies of the short GFP11 peptide and then coexpressed with excess GFP1-10 (Kamiyama *et al.* 2016; Feng *et al.* 2017). In addition to labeling the native protein with smaller covalent tags, this combinatorial approach offers the further benefit of limiting the GFP signal to the specific cell type in which GFP1-10 is expressed (Figure 1A).

In this report, we describe a NATF toolbox that combines split-GFP and CRISPR technology for live-cell imaging of labeled *Caenorhabditis elegans* proteins expressed at native levels. With this approach, a GFP11 multicopy DNA array (GFP11_{x7}) is inserted into the target gene. The resultant knock-in strain can then be crossed with separate reporter lines in which GFP1-10 is expressed in different cell types for tissue-specific visualization of the reconstituted NATF GFP (Figure 1A). We utilized this strategy for effective enhancement of an otherwise weak signal from single-copy labeling of a key protein (OIG-1) as well as the cell-specific resolution of a receptor accessory protein (LEV-10) at closely spaced but functionally distinct synapses in the *C. elegans* nervous system.

Materials and Methods

C. elegans strains

C. elegans strains were maintained at room temperature on NGM plates seeded with OP50 (Brenner 1974). Some strains were obtained from the *Caenorhabditis* Genetics Center (CGC). The N2 Bristol strain was used as the wild-type reference. Transgenic animals were generated using standard microinjection techniques (Evans 2006). Strains used in this study are described in Supplemental Material, Table S1.

Molecular biology

single-guide RNA/Cas9 plasmid design: A 200 bp DNA sequence that contained the desired cut site was submitted to the optimized CRISPR Design online tool (<http://crispr.mit.edu/>) to predict single-guide RNA (sgRNA) sequences. To enhance gene-editing efficiency, we selected a 5' N₁₈GGNGG sequence (Farboud and Meyer 2015) as an sgRNA targeting site for both *oig-1* and *lev-10*. For *oig-1*, 5'-GGAGAGAAAGACGAAAATGG-3' was cloned into pDD162 (#47549; Addgene), a plasmid that contains the sgRNA backbone and Cas9 expression system, using Q5 site-directed mutagenesis (New England Biolabs, Beverly, MA). Similarly, for *lev-10*, 5'-ACGAATCGACTGGTGCCGG-3' was used as the sgRNA target sequence, which is ~80 bp upstream of the *lev-10* stop codon.

CRISPR repair template for *oig-1* and *lev-10*: To create the Self-Excising drug selection Cassette (SEC) SEC repair template for *oig-1* TagRFP (Tag red fluorescent protein) CRISPR knock-in, flanking ~500-bp genomic DNA regions

immediately upstream and downstream of the desired insertion site were amplified by PCR using the following primers (Primer 1 and Primer 2 for the upstream homology arm, and Primer 3 and Primer 4 for the downstream homology arm) with overlap regions to the target plasmid pDD284 (#66825; Addgene):

OIG-1 Primer 1: 5'-GACGTTGTAAACGACGGCCAGTCGACCTAACCATTCCTCCAAAAGAT-3'.

OIG-1 Primer 2: 5'-TGAGTCTCTCTCCCTTGGAGACCATCGCATTATTCCTCAACTGATA-3'.

OIG-1 Primer 3: 5'-TTACAAGGATGACGATGACAAGAGAAATCTTCGCATATAGAAGA-3'.

OIG-1 Primer 4: 5'-CAGGAAACAGCTATGACCATGTTATCC AAGTCGGAGTACTGTTCA-3'.

The amplified DNA fragments were cloned into plasmid pDD284 using Gibson cloning (New England Biolabs) to create the repair template. The corresponding protospacer adjacent motif (PAM) PAM sequence in the repair template plasmid was mutated from AGG to CCC using Q5 site-directed mutagenesis to produce the final plasmid, pSH30. Correct insertions and mutations were confirmed by sequencing.

To create the SEC repair template (pSH55) for the *oig-1* GFP11_{x7} CRISPR knock-in, the GFP11_{x7} coding sequence was amplified from a previously published plasmid (#70224; Addgene) and inserted into pSH30 to replace the TagRFP sequence by In-Fusion cloning (Takara) with the following primers.

Fragment.FOR 221 5'-GTTGGAATAAATGCGATGCGTGACCACATGGTCCTT-3'.

Fragment.REV 222 5'-AAAGTACAGATTCTCGGTGATACCGGCAGCAT-3'.

Vector.FOR 223 5'-GAGAATCTGTACTTTCAATCCGGAAA GGTAAG-3'.

Vector.REV 224 5'-CGCATTTATTCCTCAACTGATAGAAAGCAT AAAAGTAGT-3'.

To create the GFP and GFP11_{x7} knock-in repair template for *LEV-10*, we used a two-step In-Fusion cloning method. Next, ~500 bp of DNA sequences upstream and downstream of the *lev-10* stop codon were selected for flanking homology arms. DNA was amplified, and then sequentially cloned into pSH30 or pSH55 to replace the original *oig-1* homology arms. The resultant plasmids were then used as templates for site-directed mutagenesis to create the final repair template plasmid with sgRNA-binding sequences mutated, pSH84 (GFP knock-in), and pSH85 (GFP11_{x7} knock-in). The primers for these cloning steps were designed with a strategy similar that used for *oig-1* as described above. Primer sequences are available on request.

GFP1-10 reporter plasmids: The DNA sequence of GFP1-10 was amplified from pcDNA3.1-GFP1-10 (#70219; Addgene) and cloned into pGH8 (*Prab-3::mCherry*) using In-Fusion cloning to create pSP1(*Prab-3::gfp1-10*). The Dorsal D (DD) and Ventral D (VD) DD and VD γ -aminobutyric acid (GABA)ergic neuron-specific promoter *Pttr-39*, the cholinergic-specific

A NATF (Native And Tissue-specific Fluorescence)

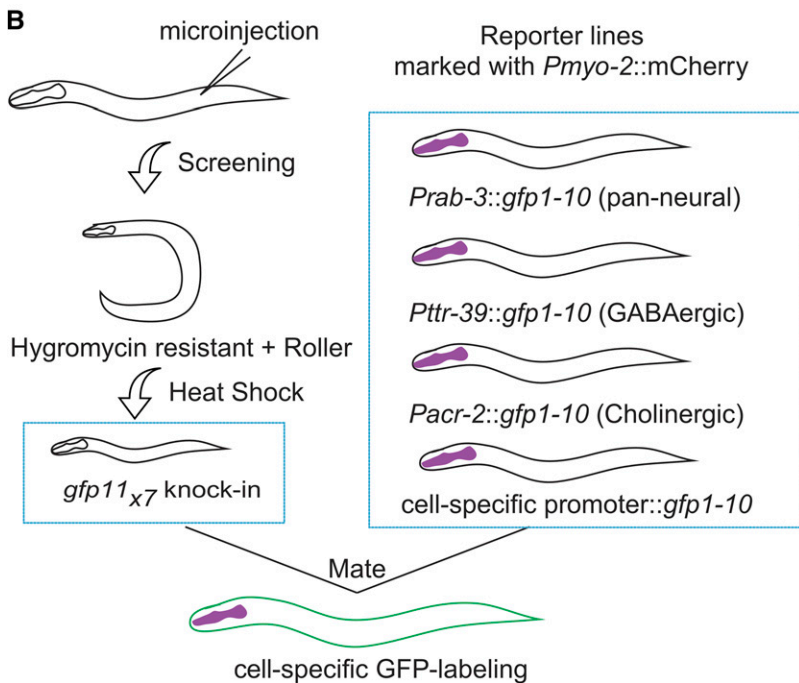
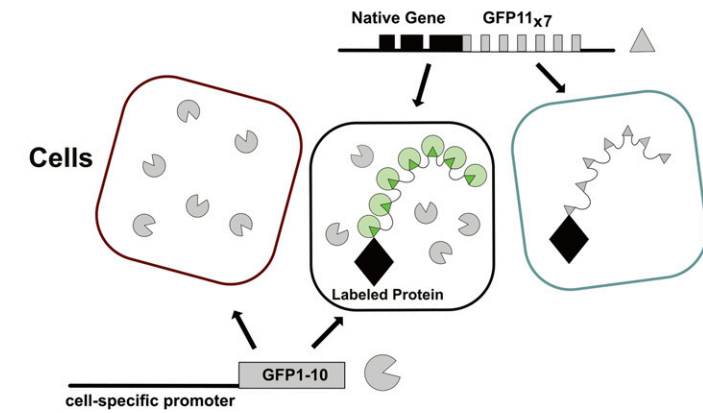


Figure 1 Robust, tissue-specific labeling of a target protein at its native expression level. (A) NATF. CRISPR/Cas9-mediated gene editing is used to label a protein of interest with seven copies of GFP11 (GFP11_{x7}). Transgenic expression of GFP1-10 with cell-specific promoters results in a bright, stable NATF fluorescent signal from multiple, reconstituted GFP molecules in specific tissues. (B) NATF workflow. Worms are injected with sgRNA, repair template, and co-injection markers. *gfp11_{x7}* knock-in worms are recovered after heat shock-induced excision of positive-selection genes. Crossing the *gfp11_{x7}* knock-in with *gfp1-10* reporter lines results in tissue-specific labeling of the target protein with a reconstituted NATF-GFP tag. CRISPR, clustered regularly interspaced short palindromic repeats; GABA, γ -aminobutyric acid; NATF, Native And Tissue-specific Fluorescence; sgRNA, single-guide RNA.

promoter *Pacr-2*, and the muscle-specific *Pmyo-3* promoter were amplified to replace the *Prab-3* promoter in pSP1 to create pSH79 (*Pptr-39::gfp1-10*), pSH88 (*Pacr-2::gfp1-10*), pSH86 (*Pmyo-3::gfp1-10*), and pSH87 (*Pflp-13::gfp1-10*). To create a secreted GFP1-10 construct, In-Fusion cloning was used to add the first 114 bp of the *oig-1* sequence including the signal sequence (Philbrook *et al.* 2018) prior to the start codon of GFP1-10 in pSP1. The combined sequence was analyzed using the SignalP 4.1 Server to confirm that the predicted signal peptide was intact. The final plasmid, pSH69 (*Prab-3::ssGFP1-10*), was confirmed by sequencing.

Confocal microscopy and image processing

Fluorescent images were captured at room temperature using a Nikon (Garden City, NY) A1R confocal microscope. Nematodes were immobilized with 15 mM levamisole/0.05%

tricaine on a 2% agarose pad in M9 buffer. All images for ACR-12::GFP fluorescence quantification were obtained with the same settings using a 40 \times /1.4 oil objective and Nyquist sampling. Constant laser power was used to compare the LEV-10::GFP fluorescence intensity to that of the NATF GFP signal produced by the combination of LEV-10::GFP11_{x7} with *Pmyo-3::GFP1-10*. Images in Figure 4 were three-dimensionally deconvolved with NIS-Elements with the automatic algorithm. For other images, ND2 files generated with NIS-Elements were imported into Fiji for analysis. Maximum intensity projections were generated by selecting stacks that had both ventral and dorsal signals. Line scans of dorsal and ventral cords (Figure S2, B–D), and of the nerve ring (Figure 3C), were adjusted by subtraction of background fluorescence measured from an adjacent region for comparison of fluorescence intensities between samples. To compare the stability of GFP signals in *lev-10::gfp* vs. *lev-10::gfp11_{x7}*;

Pmyo-3::GFP1-10 strains, a region of interest (ROI) of the same size in each strain was bleached with a 405-nm laser for 15 sec at 50% laser power. Images of the ROI were collected and compared, before and after photobleaching. *OIG-1::GFP11_{x7}* and *mCherry::OIG-1* strains were imaged using an A1R Nikon laser confocal to obtain intensity profiles (Figure 2A and Figure S3). Fiji was used to draw 15- μ m long-line scans on the ventral cord and extract intensity profiles, which were exported to Excel. Fluorescent intensities were normalized to the maximum intensity value of each line scan. Intensities were plotted using Prism 6 software. Peaks exceeding a threshold of 75% of the normalized intensity for each sample were counted.

AiryScan imaging

Worms were mounted on 10% agarose pads and immobilized with 15 mM levamisole/0.05% tricaine dissolved in M9. A Zeiss ([Carl Zeiss], Thornwood, NY) LSM880 microscope equipped with an AiryScan detector and a 63 \times /1.40 Plan-Apochromat oil objective lens was used to acquire superresolution images of the DD neuron (Figure 4E). Images were acquired as a Z-stack (0.19 μ m/step), spanning the total volume of the DD neuron and submitted for AiryScan image processing by ZEN software.

Statistical analysis

For all experiments, sample numbers were $n > 10$. The Student's *t*-test was used for comparison between two groups. $P < 0.05$ was considered significant. Prism 6 was used for statistical analysis.

Immunoblotting

OIG-1 CRISPR and transgenic overexpression strains were cultured on NGM plates seeded with OP50. Mixed-stage worms were collected into a 1.5-ml tube by washing them off NGM plates with M9 buffer and pelleted by centrifugation. Next, 50 μ l of 2 \times SDS-PAGE protein sample buffer was added to a 50 μ l pellet of each genotype and heated to 90 $^\circ$ for 15 min. Samples were centrifuged at 8000 rpm for 5 min to remove debris (Miller *et al.* 1983). Then, 30 μ l of supernatant from each genotype was loaded on a 10% protein gel to run at 110 V for 60 min, before being transferred to a PVDF membrane for immunoblot analysis (Duerr 2006). Immunoblots were treated with monoclonal anti-FLAG M2 antibody (1:500) (Sigma [Sigma Chemical], St. Louis, MO) to the 3XFLAG peptide followed by HRP-conjugated goat anti-mouse IgG antibody (1/2000), and soaked for 2 min in developing solution for chemiluminescent detection (Alegria-Schaffer *et al.* 2009).

Data availability

All reagents and *C. elegans* strains described in this work are available on request. Plasmids will be deposited at Addgene and *C. elegans* strains submitted to the CGC stock center. Supplemental figures have been uploaded at the Genetics Society of America Figshare portal. Supplemental material available at <https://doi.org/10.25386/genetics.7898075>.

Results

Tool box and strategy for NATF GFP labeling

We used a previously described CRISPR/Cas9 system for genome editing in *C. elegans* (Dickinson *et al.* 2015). In this approach, homology arms flank a self-excising cassette that carries positive selection markers (*sqt-1*) for the identification of transgenic worms ("rollers") and drug resistance (*hygR*) for the detection of CRISPR/Cas9-induced integrants. A brief heat-shock treatment induces excision of the marker cassette to restore wild-type movement ("nonroller") (Figure 1B). For split-GFP experiments, we replaced the fluorescent protein sequence in the original repair template plasmid with a *gfp11_{x7}* insert (Kamiyama *et al.* 2016). Homology arms of \sim 500 bp were used for the two genes targeted (*oig-1* and *lev-10*) in this study (Figure S1A). We also constructed separate plasmids for expressing GFP1-10 in specific cell types including body muscles, all neurons, cholinergic neurons, and GABAergic neurons (Figure 1B and Figure S1B). In these lines, the GFP1-10 transgenes are carried as extrachromosomal arrays that are maintained by selecting for a pharyngeal co-injection marker (*Pmyo-2::mCherry*) (Figure 1B). Cell-specific drivers are flanked with multiple cloning sites to facilitate the construction of plasmids for GFP1-10 expression in other tissues (Figure S1B). *gfp11_{x7}* knock-in strains can be confirmed within 2 weeks of the initial injection and then crossed with GFP1-10-expressing lines for characterization (Figure 1B).

NATF GFP labeling reveals the intracellular localization of *OIG-1* in GABAergic motor neurons

oig-1 encodes a soluble protein with a single immunoglobulin domain (Figure 2B) that is temporally regulated in GABAergic motor neurons to antagonize a synaptic remodeling program; in *oig-1* mutants, a postsynaptic acetylcholine receptor (AChR) containing the AChR subunit, ACR-12::GFP, is ectopically relocated from dorsal to ventral GABAergic neuron processes. *OIG-1* is secreted when overexpressed from multicopy transgenic arrays to produce bright puncta adjacent to clusters of ACR-12::GFP (Figure 2, A and B) (He *et al.* 2015; Howell *et al.* 2015). To ask if *OIG-1* is also secreted when expressed from the native locus, we used CRISPR/Cas9 to engineer a single-copy knock-in of the TagRFP together with a 3XFLAG epitope tag (Figure 2B and Figure S2, A–C). We used immunoblotting to confirm expression of TagRFP::3XFLAG::*OIG-1* (Figure 2C) but failed to detect TagRFP expression *in vivo* either by TagRFP fluorescence (Figure 2, D–G) or by immunostaining against the 3XFLAG epitope (data not shown). To produce a potentially brighter signal, we created a *gfp11_{x7}::oig-1* knock-in (Figure 2B) with a sgRNA that targeted the same 5'-N₁₈GGNGG site used for the TagRFP insert (Farboud and Meyer 2015). This strategy was designed to enhance a potential fluorescent signal by attaching seven copies of the GFP11 peptide to the *OIG-1* N-terminus (Kamiyama *et al.* 2016). Successful knock-in of *gfp11_{x7}* was confirmed by sequencing (data not shown).

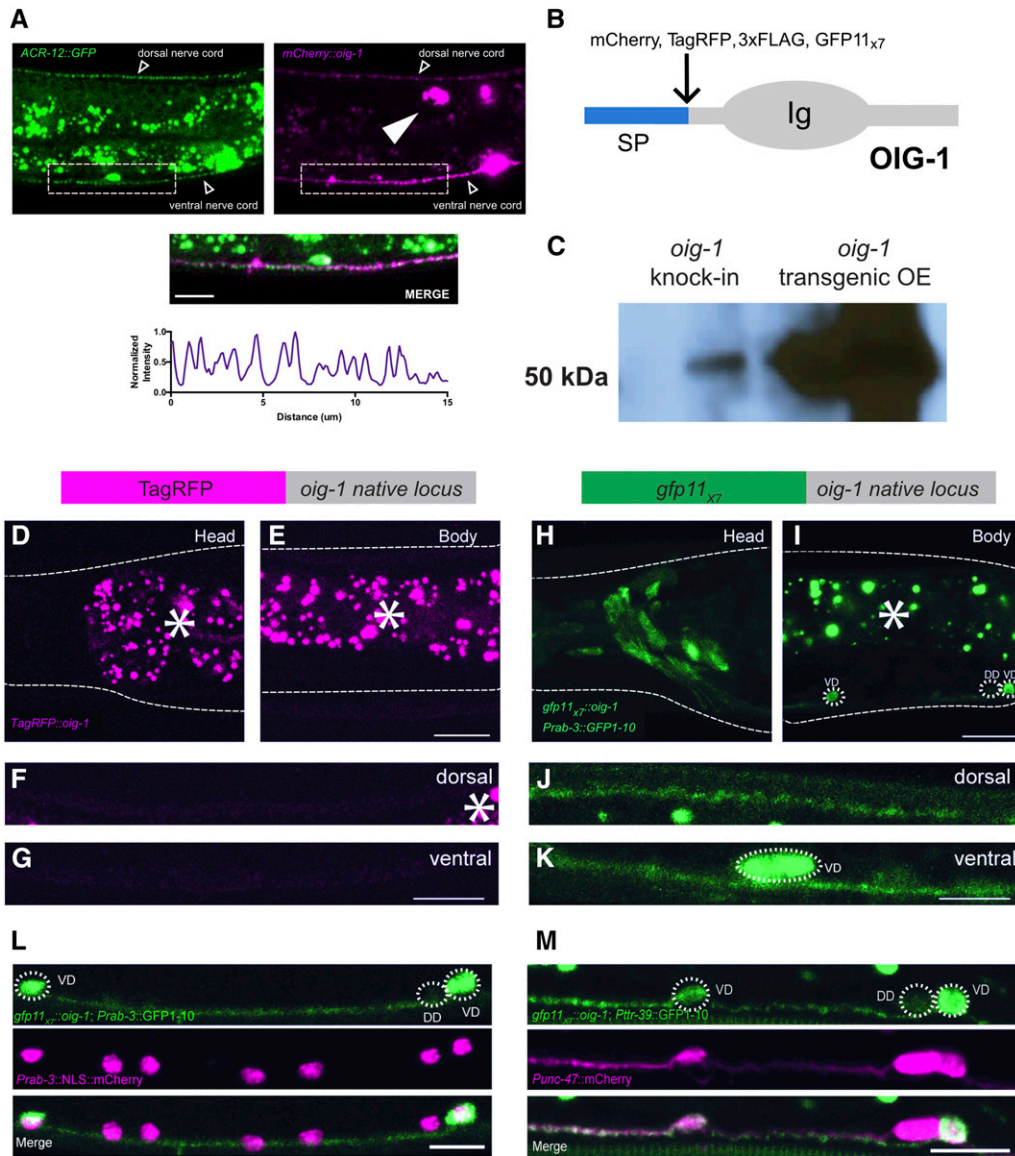


Figure 2 CRISPR knock-in of GFP11_{x7} in OIG-1 reveals its intracellular localization in GABAergic motor neurons. (A) Overexpression of mCherry::OIG-1 from a transgenic array (*Punc-25::mCherry::oig-1*) produces bright puncta (magenta) adjacent to ACR-12::GFP-labeled postsynaptic clusters (green) of AChRs in GABAergic motor neurons (*Punc-47::acr-12::gfp*). Merge shows ventral nerve cord. Bar, 10 μ m. Line scan of mCherry::OIG-1 in the ventral nerve cord (bottom) shows punctate signal. Arrowhead points to coelomocyte. (B) OIG-1 protein showing N-terminal SP, C-terminal Ig (Immunoglobulin) domain, and insertion site for fluorescent and epitope tags (mCherry, TagRFP, 3xFLAG, and GFP11_{x7}). (C) Immunoblot stained for the 3XFLAG tag detects expression of single-copy TagRFP::OIG-1 knock-in and confirms over expression of mCherry::3XFLAG::OIG-1 from multicopy transgenic array. (D–G) TagRFP knock-in at the *oig-1* locus (top) does not result in detectable TagRFP::OIG-1 fluorescence. Note absence of TagRFP::OIG-1 signal in head neurons (D), body (E), and dorsal (F) and ventral (G) nerve cords. Asterisks mark autofluorescent granules. (H–K) OIG-1 expression in the nervous system. The *gfp11_{x7}::oig-1* knock-in (top) was crossed with the pan-neuronal transgenic line expressing *Prab-3::GFP1-10*. A diffuse OIG-1 NATF GFP signal is detected in head neurons (H) and in VD but not DD GABAergic motor neuron

cell soma (dashed outlines) in the ventral cord (I). NATF GFP-labeled OIG-1 is detectable in both dorsal and ventral nerve cords (J and K). Asterisk marks autofluorescent granules. (L and M) OIG-1 expression in the nervous system and in GABAergic motor neurons. (L) The *gfp11_{x7}::oig-1* knock-in line was crossed with the pan-neuronal marker *Prab-3::gfp1-10* and all neurons labeled with a nuclear-localized pan-neuronal label, *Prab-3::NLS::mCherry*. Note OIG-1 NATF GFP signal specifically in VD but not DD cell soma (dashed outlines), nor in additional ventral cord *Prab-3::NLS::mCherry*-labeled nuclei corresponding to cholinergic motor neurons. (M) The *gfp11_{x7}::oig-1* knock-in was crossed with the GABAergic motor neuron-specific marker *Pttr-39::gfp1-10* and all GABA neurons were labeled with *Punc-47::mCherry*. Note the OIG-1 NATF GFP signal in VD but not DD motor neurons (dashed outlines)¹⁴. GFP1-10 is cytosolically expressed from the *Prab-3::gfp1-10* and *Pttr-39::gfp1-10* transgenes, thus indicating that OIG-1 is intracellularly localized at its native expression level. All fluorescent images were obtained from L4-stage larvae. Bar, 10 μ m. AChR, acetylcholine receptor; CRISPR, clustered regularly interspaced short palindromic repeats; DD, Dorsal D neuron; GABA, γ -aminobutyric acid; NATF, Native And Tissue-specific Fluorescence; SP, signal peptide; TagRFP, Tag red fluorescent protein; VD, Ventral D neuron.

We have previously shown that ACR-12::GFP in VD-class GABAergic motor neurons mislocalizes to the ventral side in *oig-1* mutants, thereby resulting in an asymmetric ACR-12::GFP signal that is brighter in the ventral vs. dorsal nerve cords (Figure S2) (He *et al.* 2015). In contrast, in the wildtype, ACR-12::GFP puncta are evenly distributed between dorsal and ventral nerve cords. This symmetry is maintained in the *gfp11_{x7}::oig-1* strain, thus arguing that the GFP11_{x7} adduct does not significantly disrupt OIG-1 function (Figure S2, C and D). We then crossed the *gfp11_{x7}::oig-1* knock-in with a pan-neuronal

Prab-3::gfp1-10 transgenic line. Consistent with our previous findings, the OIG-1 NATF GFP signal can be detected in head neurons, and in both dorsal and ventral nerve cords (Figure 2, H–K) (He *et al.* 2015). Colocalization of OIG-1 NATF GFP with the nuclear-localized pan-neuronal marker *Prab-3::NLS::mCherry* confirmed OIG-1 expression in neurons (Figure 2L). As an independent strategy to validate OIG-1 expression in GABA neurons, we crossed the *gfp11_{x7}::oig-1* line with *Pttr-39::gfp1-10*, which is selectively expressed in DD- and VD-class GABAergic motor neurons (Cinar *et al.* 2005). In

In this case, the **OIG-1** NATF GFP signal is limited to VD neurons with either weak or undetectable expression in DD neurons in L4 larvae (Figure 2M). This finding confirms previous results obtained with a *Poig-1::gfp* transcriptional reporter that was expressed in VD, but not DD, neurons after the L2 larval stage (He *et al.* 2015). Because the GFP1-10 peptide is expressed intracellularly in these strains, the NATF GFP signal likely derives from cytoplasmic **OIG-1**. Notably, the **OIG-1** NATF GFP signal is visible throughout VD neuron soma and neurites (Figure 2, H–M), and does not show the distinctive highly punctate appearance of **OIG-1** when overexpressed from a multicopy array (Figure 2A) (Figure S3) (He *et al.* 2015; Howell *et al.*, 2015). To test for potential secretion of **OIG-1** from the native locus, the *gfp11_{x7}::oig-1* knock-in was crossed with a transgenic line in which the GFP1-10 peptide is secreted from neurons (*Prab-3::ss::gfp1-10*). However, this experiment did not produce a detectable extracellular NATF signal nor GFP fluorescence in coelomocytes in the body cavity, which normally function as macrophage-like cells and thus can be used to detect secreted protein markers (Figure S4A) (Fares and Greenwald 2001). Notably, overexpression of mCherry::**OIG-1** from an extrachromosomal array does label coelomocytes (He *et al.* 2015; Howell *et al.* 2015). As a positive control, we showed that the secreted form of GFP1-10 in the *Prab-3::ss::gfp1-10* strain is functional because it robustly labels a GFP11 peptide fused to the extracellular domain of the synaptic membrane protein **NLG-1** (Feinberg *et al.* 2008) (Figure S4, B–D). As negative controls, we showed that neither GFP11_{x7} nor GFP1-10 by themselves produce visible GFP fluorescence (Figure S2, E and F). Although undetectably low levels of secreted **OIG-1** could be produced by this experiment, our overall results are consistent with the hypothesis that **OIG-1** is not secreted when expressed at the native level but localizes intracellularly (S. He, A. Cuentas Condori, D. Miller, unpublished data). For example, genetic disruption of the **OIG-1** signal peptide blocks **OIG-1** secretion but does not disrupt *oig-1* function *in vivo* (He *et al.* 2015). Our finding that **OIG-1** is intracellularly localized depended on the use of the NATF strategy to reveal low levels of native **OIG-1** expression and thereby circumvent artifactual extracellular localization due to **OIG-1** overexpression from multicopy arrays (He *et al.* 2015).

NATF GFP labeling reveals discrete locations for the transmembrane domain protein LEV-10 in different cell types

Having shown that NATF could detect a soluble protein (**OIG-1**), we next targeted **LEV-10**, a CUB domain transmembrane protein that clusters AChRs at postsynaptic sites in body muscles (Gally *et al.* 2004). First, we created a CRISPR/Cas9 knock-in line in which a single copy of GFP was fused to the intracellular C-terminus of **LEV-10** (see Figure 4A). We detected **LEV-10::GFP** in both ventral and dorsal nerve cords, as predicted for a protein that localizes to body muscle synapses (Gally *et al.* 2004). **LEV-10::GFP** puncta were also detected in the head region where motor neurons synapse with

body muscles on the inside surface of the nerve ring (White *et al.* 1986; Von Stetina *et al.* 2006) (Figure 3A). For NATF GFP labeling of body muscle synapses, we generated a *lev-10::gfp11_{x7}* knock-in and crossed it with a muscle-specific line expressing GFP1-10 (*Pmyo-3::gfp1-10*) from an extrachromosomal array. The **LEV-10** muscle-specific NATF GFP signal in the head region and axial nerve cords (Figure 3B) mimics that of the single-copy *lev-10::gfp* knock-in (Figure 3A), but is noticeably brighter. We quantified the GFP signal for each marker at the nerve ring muscle synapses to confirm that the **LEV-10** NATF fluorescence is brighter (around three times) than the GFP signal from the *lev-10::gfp* single-copy insertion, as predicted from measurements of single-copy vs. multicopy split-GFP expressed in cultured cells (Figure 3C) (Kamiyama *et al.* 2016). In addition to determining that the *lev-10::gfp11_{x7}* array yields a stronger signal than that of the single-copy *lev-10::GFP* insert, we also showed that NATF GFP is substantially more resistant to photobleaching, as previously demonstrated for reconstituted split-GFP from measurements *in vitro* (Kamiyama *et al.* 2016) (Figure 3D).

In addition to expression in muscle, our independent studies have shown that **LEV-10** is also expressed in ventral cord neurons where it colocalizes with AChRs at postsynaptic sites in GABAergic motor neurons (S. He, A. Cuentas Condori, D. Miller, unpublished data). In the motor neuron circuit, cholinergic motor neurons form dyadic synapses that innervate closely spaced postsynaptic domains in body muscle and GABA neurons (see Figure 4G) (White *et al.* 1986). Both of these postsynaptic regions in the ventral nerve cord region should be labeled in the *lev-10::gfp* knock-in and, thus, cannot be unambiguously identified (Figure 3A). To resolve this problem, we crossed the *lev-10::gfp11_{x7}* knock-in with transgenic lines that express GFP1-10 in either body muscles (*Pmyo-3::gfp1-10*), or in DD and VD GABAergic motor neurons (*Pttr-39::gfp1-10*). NATF GFP puncta can be readily detected in both cases (Figure 4, C and D), but are brighter in muscles than in GABAergic neurons (data not shown). Expression of a TagRFP-labeled AChR subunit **UNC-29** (Gally *et al.* 2004) in muscle confirms colocalization of **UNC-29::TagRFP** with **LEV-10** NATF GFP reconstituted in muscle. (Figure 4C). Expression of GFP1-10 in DD and VD neurons produces **LEV-10** NATF GFP puncta that overlap with a cytoplasmic GABA neuron mCherry marker (*Punc-47::mCherry*), as predicted for the **LEV-10** protein that localizes to GABA neuron synapses (Figure 4D). To confirm the postsynaptic location of **LEV-10** in GABA neurons, we used a DD-specific construct (*Pflp-13::gfp1-10*) to generate a **LEV-10** NATF GFP signal. In this case, superresolution imaging resolves distinct **LEV-10** NATF GFP puncta at the tips of postsynaptic spine-like projections that have been recently described in the ventral processes of mature DD neurons (Figure 4E) (Philbrook *et al.* 2018). Notably, we have also observed that the AChR marker, **ACR-12::GFP**, is positioned in the same distal location in DD dendritic spines and that these spines are aligned with presynaptic cholinergic vesicles (Cuentas-Condori *et al.* 2019) (Philbrook *et al.* 2018). In addition to resolving

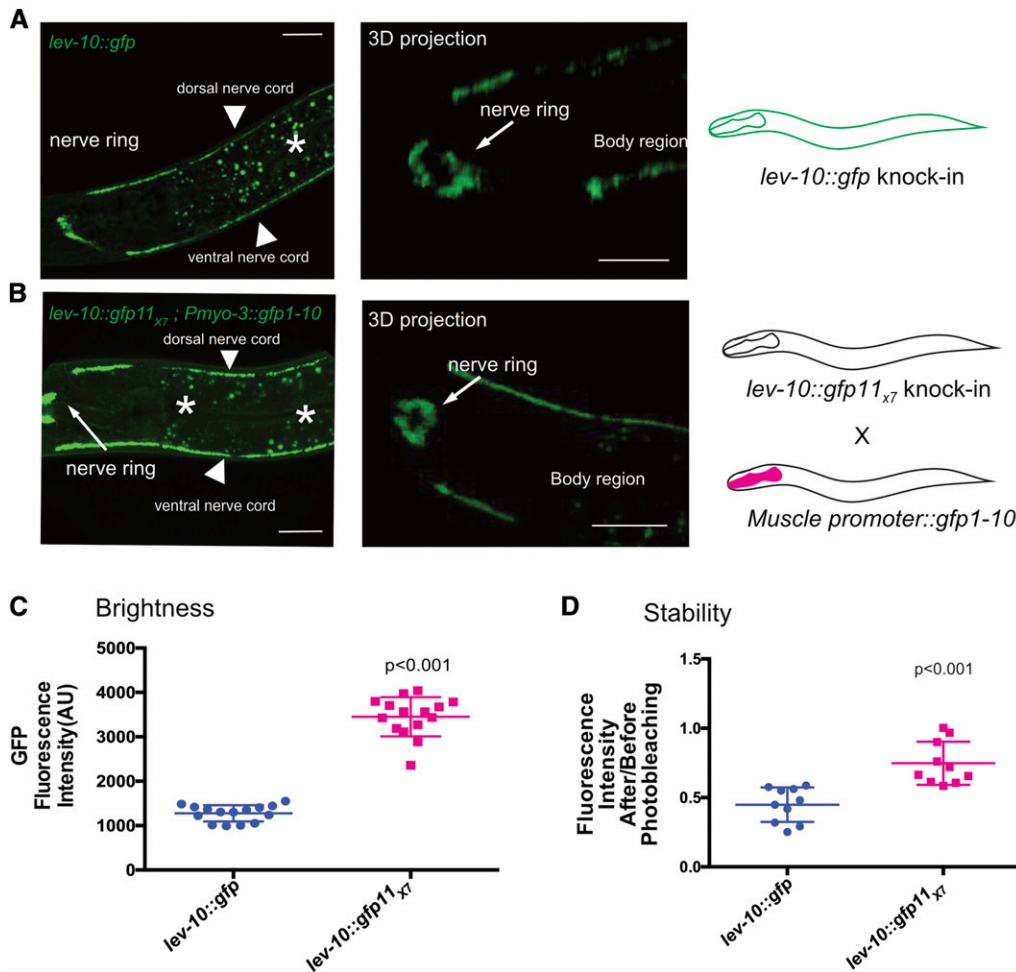


Figure 3 *lev-10::gfp11_{x7}* yields a stronger NATF GFP signal than the single-copy *lev-10::gfp* knock-in at synapses in neurons and muscle cells. (A) Confocal image showing localization of LEV-10::GFP in a single-copy GFP knock-in at the native *lev-10* gene (*lev-10::gfp*). LEV-10::GFP puncta are visible at the nerve ring (arrow), and in ventral and dorsal nerve cords (arrowheads). (B) Confocal image of the LEV-10 NATF GFP signal at body muscle synapses arising from the combination of the *lev-10::gfp11_{x7}* knock-in with *Pmyo-3::gfp1-10*. NATF GFP (arrow) is detected at neuromuscular synapses near the nerve ring. Bar, 20 μ m. Insets (right) shows rotated views of anterior regions of images on left to depict nerve ring labeling. Asterisks mark gut autofluorescence. (C) LEV-10 NATF GFP at body muscle synapses in the nerve ring labeled with *lev-10::gfp11_{x7}* is significantly brighter (around three times) (3450 ± 441) than the single-copy *lev-10::gfp* knock-in (1280 ± 184). $P < 0.001$, $N = 15$, Student's *t*-test. Error bars are SD. (D) The LEV-10 NATF GFP signal at body muscle synapses in the nerve ring labeled with *lev-10::gfp11_{x7}* is significantly more stable (0.75 ± 0.15) to photobleaching than the single-copy *lev-10::gfp* knock-in in

the nerve ring (0.45 ± 0.12), $N = 10$, $P < 0.001$, Student's *t*-test. See *Materials and Methods*. Error bars are SD. AU, arbitrary units; NATF, Native And Tissue-specific Fluorescence.

LEV-10 localization at distinct postsynaptic locations in muscle vs. GABA neurons, we also used a cholinergic motor neuron driver (*Pacr-2::gfp1-10*) to detect a separate LEV-10 NATF signal in ventral cord cholinergic neurons. In this case, LEV-10 NATF GFP is diffuse (Figure 4F) and asymmetrically localized to the ventral, but not dorsal, nerve cord (data not shown), a labeling pattern that closely resembles the perisynaptic position of the AChR subunit ACR-12::GFP in cholinergic motor neurons (Petrash *et al.* 2013). Because LEV-10 is expressed at its native level and retains its AChR clustering function (data not shown) when fused to the GFP11_{x7} adduct, it seems likely that each of the three distinct, cell-specific LEV-10 NATF signals (*i.e.*, muscle, GABA neurons, and cholinergic neurons) marks authentic subcellular locations for the endogenously expressed LEV-10 protein.

Discussion

We have shown that NATF offers a robust strategy for producing bright, cell-specific signals for the *C. elegans* proteins OIG-1 and LEV-10 expressed from their native genomic loci. These results suggest that NATF should be especially useful

for marking connections in the compact *C. elegans* nervous system, where most synapses are located in the densely packed nerve ring and axial nerve cords (White *et al.* 1986). For example, GFP-tagging of a core presynaptic protein (*e.g.*, RAB-3) by conventional CRISPR/Cas9 editing should mark synapses throughout the nervous system. In contrast, labeling with the NATF strategy should result in a bright, photostable GFP signal that is limited to the presynaptic domains of specific neurons. Although our results have determined that fusion with the GFP11_{x7} peptide does not result in detectable disruption of the *in vivo* function of either OIG-1 (Figure S2, B–D) or LEV-10 (Figure 4C and S. (S. He, A. Cuentas Condori, D. Miller, unpublished data), other proteins may be less tolerant. In that event, smaller adducts with fewer copies of GFP11 could be attempted. In that case, GFP signal augmentation will be diminished but tissue-specific labeling is still possible (Noma *et al.* 2017). Because the *gfp11_{x7}* insert is stably integrated at the native locus and is thus limiting, the complementing GFP1-10 peptide can be provided from multicopy transgenic arrays without risk of inducing overexpression artifacts. Thus, a given GFP11_{x7} split GFP insert can be rapidly tested with multiple tissue-specific GFP1-10 transgenic lines,

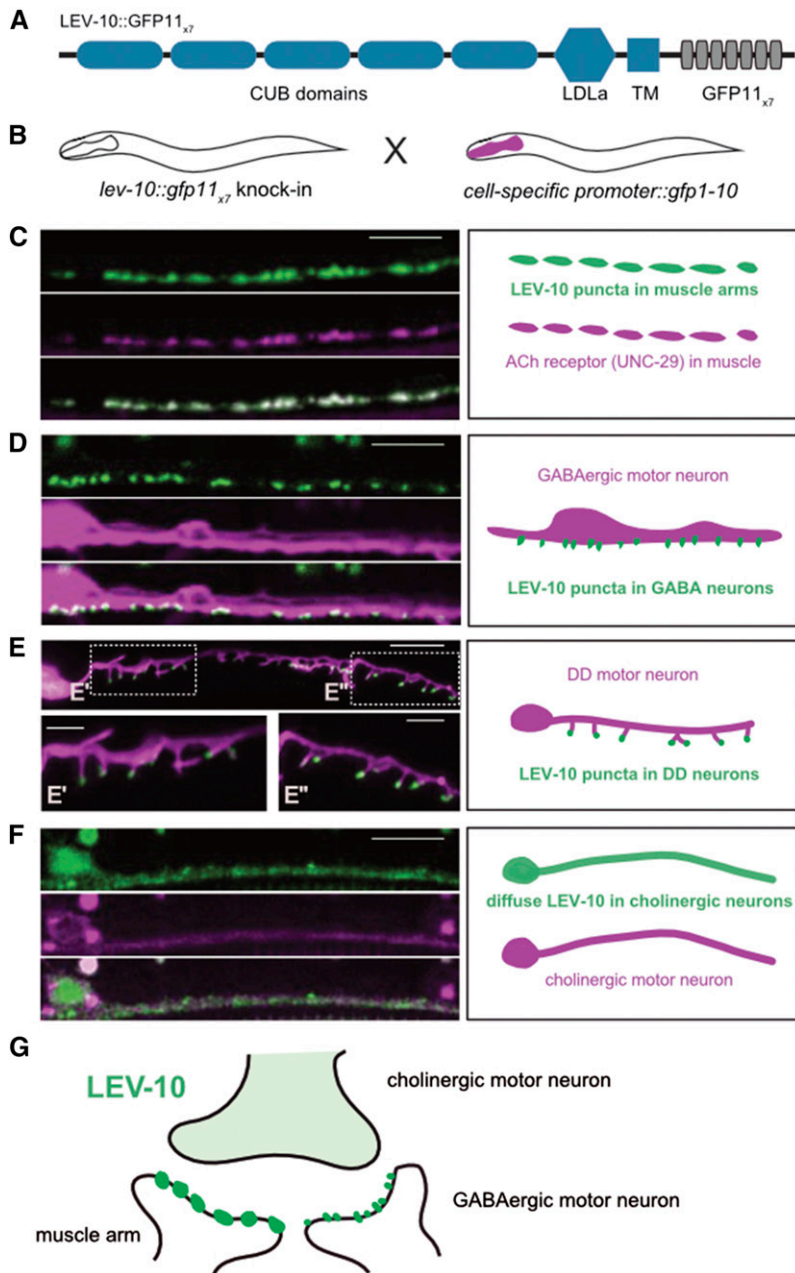


Figure 4 Visualization of LEV-10 NATF GFP signal at cell-specific synapses. (A) Schematic of LEV-10::GFP11_{x7} showing extracellular complement C1r/C1s, Uegf, Bmp1 (CUB) CUB and low-density lipoprotein receptor domain class A (LDLa) LDLa domains, with TM region and cytoplasmic tail with GFP11_{x7} insert. (B) Cell-specific labeling strategy. The *lev-10::gfp11_{x7}* knock-in strain is crossed with separate transgenic lines expressing GFP1-10 in specific cell types. (C–F) Representative images (left) and schematics (right) of ventral nerve cord region of L4 larvae showing LEV-10 NATF GFP arising from complementation of the *lev-10::gfp11_{x7}* knock-in with cell-specific expression of GFP1-10: (C) *Pmyo-3::gfp1-10* (body muscle), (D) *Pptr-39::gfp1-10* (DD and VD GABAergic motor neurons), (E) *Pflp-13::gfp1-10* (DD GABAergic motor neurons) with superresolution images with insets (E' and E'') showing localization of LEV-10 NATF GFP to tips of postsynaptic DD dendritic spines, and (F) *Pacr-2::gfp1-10* (cholinergic motor neurons). *Pmyo-3::unc-29::TagRFP* marks ACh receptors in body muscle in (C), *Punc-47::mCherry* labels GABA neurons in (D), *Pflp-13::LifeAct::mCherry* marks DD neurons in (E), and *Punc-4::mCherry* labels cholinergic motor neurons in (F). Bars, 5 (C–F) and 2 μm (E' and E''). (G) Schematic showing distribution of LEV-10 NATF GFP at a dyadic synapse of a presynaptic cholinergic motor neuron with postsynaptic body muscle and GABAergic motor neuron in the ventral nerve cord. ACh, acetylcholine; DD, Dorsal D neuron; GABA, γ-aminobutyric acid; NATF, Native And Tissue-specific Fluorescence; TagRFP, Tag red fluorescent protein; TM, transmembrane; VD, Ventral D neuron.

which can be readily generated using conventional methods. A similar combinatorial approach should also be useful for tissue-specific protein labeling in other model organisms (Kelliher *et al.* 2018). We note that NATF can be modified to reduce weak background fluorescence from the GFP1-10 fragment (Feng *et al.* 2017), and for multicolor split-GFP imaging with cyan (CFP) and yellow (YFP) GFP variants, or with the *sfmCherry* marker (Kamiyama *et al.* 2016; Feng *et al.* 2017).

Acknowledgments

We thank members of the Miller laboratory for critical reading of the manuscript, Sierra Palumbos and Alice Siqi Chen for

plasmid construction, Lakshmi Sundararajan for help with confocal imaging, and Oliver Hobert for sharing strains. Some nematode strains used in this work were provided by the *Caenorhabditis* Genetics Center, which is funded by the National Institutes of Health (NIH) National Center for Research Resources. Superresolution images were acquired in the Vanderbilt Cell Imaging Shared Resource (1S10 OD-201630-01). This work was supported by NIH grants to D.M.M. (R01 NS-081259 and R01 NS-106951). A.C.-C. is supported by an American Heart Association predoctoral fellowship (18PRE33960581).

Author contributions: S.H., A.C.-C., and D.M.M. conceived the project. S.H. and A.C.-C. performed the experiments and analyzed the data. S.H., A.C.-C., and D.M.M. wrote the manuscript. The authors declare no competing interests.

Literature Cited

- Alegria-Schaffer, A., A. Lodge, and K. Vattem, 2009 Performing and optimizing Western blots with an emphasis on chemiluminescent detection. *Methods Enzymol.* 463: 573–599. [https://doi.org/10.1016/S0076-6879\(09\)63033-0](https://doi.org/10.1016/S0076-6879(09)63033-0)
- Brenner, S., 1974 The genetics of *Caenorhabditis elegans*. *Genetics* 77: 71–94.
- Cabantous, S., T. C. Terwilliger, and G. S. Waldo, 2005 Protein tagging and detection with engineered self-assembling fragments of green fluorescent protein. *Nat. Biotechnol.* 23: 102–107. <https://doi.org/10.1038/nbt1044>
- Chalfie, M., 2009 GFP: lighting up life. *Proc. Natl. Acad. Sci. USA* 106: 10073–10080. <https://doi.org/10.1073/pnas.0904061106>
- Cinar, H., S. Keles, and Y. Jin, 2005 Expression profiling of GABAergic motor neurons in *Caenorhabditis elegans*. *Curr. Biol.* 15: 340–346. <https://doi.org/10.1016/j.cub.2005.02.025>
- Cuentas-Condori, A., B. Mulcahy, S. He, S. Palumbos, M. Zhen *et al.*, 2019 Dendritic spines on GABAergic neurons respond to cholinergic signaling in the *Caenorhabditis elegans* motor circuit. *bioRxiv*. Available at: <https://www.biorxiv.org/content/10.1101/598714v2>.
- Dickinson, D. J., A. M. Pani, J. K. Heppert, C. D. Higgins, and B. Goldstein, 2015 Streamlined genome engineering with a self-excising drug selection cassette. *Genetics* 200: 1035–1049. <https://doi.org/10.1534/genetics.115.178335>
- Duerr, J. S., 2006 Immunohistochemistry (June 19, 2006), *WormBook* ed. The *C. elegans* Research Community, *WormBook*, doi/10.1895/wormbook.1.105.1, <http://www.wormbook.org>.
- El Mouridi, S., C. Lecroisey, P. Tardy, M. Mercier, A. Leclercq-Blondel *et al.*, 2017 Reliable CRISPR/Cas9 genome engineering in *Caenorhabditis elegans* using a single efficient sgRNA and an easily recognizable phenotype. *G3 (Bethesda)* 7: 1429–1437. <https://doi.org/10.1534/g3.117.040824>
- Evans, T. C., 2006 Transformation and microinjection (April 6, 2006), *WormBook*, ed. The *C. elegans* Research Community, *WormBook*, doi/10.1895/wormbook.1.108.1, <http://www.wormbook.org>.
- Farboud, B., and B. J. Meyer, 2015 Dramatic enhancement of genome editing by CRISPR/Cas9 through improved guide RNA design. *Genetics* 199: 959–971. <https://doi.org/10.1534/genetics.115.175166>
- Fares, H., and I. Greenwald, 2001 Genetic analysis of endocytosis in *Caenorhabditis elegans*: coelomocyte uptake defective mutants. *Genetics* 159: 133–145.
- Feinberg, E. H., M. K. Vanhoven, A. Bendesky, G. Wang, R. D. Fetter *et al.*, 2008 GFP reconstitution across synaptic partners (GRASP) defines cell contacts and synapses in living nervous systems. *Neuron* 57: 353–363. <https://doi.org/10.1016/j.neuron.2007.11.030>
- Feng, S., S. Sekine, V. Pessino, H. Li, M. D. Leonetti *et al.*, 2017 Improved split fluorescent proteins for endogenous protein labeling. *Nat. Commun.* 8: 370. <https://doi.org/10.1038/s41467-017-00494-8>
- Gally, C., S. Eimer, J. E. Richmond, and J.-L. Bessereau, 2004 A transmembrane protein required for acetylcholine receptor clustering in *Caenorhabditis elegans*. *Nature* 431: 578–582. <https://doi.org/10.1038/nature02893>
- He, S., A. Philbrook, R. McWhirter, C. V. Gabel, D. G. Taub *et al.*, 2015 Transcriptional control of synaptic remodeling through regulated expression of an immunoglobulin superfamily protein. *Curr. Biol.* 25: 2541–2548. <https://doi.org/10.1016/j.cub.2015.08.022>
- Hostettler, L., L. Grundy, S. Käser-Pébernard, C. Wicky, W. R. Schafer *et al.*, 2017 The bright fluorescent protein mNeonGreen facilitates protein expression analysis in vivo. *G3 (Bethesda)* 7: 607–615. <https://doi.org/10.1534/g3.116.038133>
- Howell, K., J. G. White, and O. Hobert, 2015 Spatiotemporal control of a novel synaptic organizer molecule. *Nature* 523: 83–87. <https://doi.org/10.1038/nature14545>
- Hsu, P. D., E. S. Lander, and F. Zhang, 2014 Development and applications of CRISPR-Cas9 for genome engineering. *Cell* 157: 1262–1278. <https://doi.org/10.1016/j.cell.2014.05.010>
- Kamiyama, D., S. Sekine, B. Barsi-Rhyne, J. Hu, B. Chen *et al.*, 2016 Versatile protein tagging in cells with split fluorescent protein. *Nat. Commun.* 7: 11046. <https://doi.org/10.1038/ncomms11046>
- Kelliher, M. T., Y. Yue, A. Ng, D. Kamiyama, B. Huang *et al.*, 2018 Autoinhibition of kinesin-1 is essential to the dendrite-specific localization of Golgi outposts. *J. Cell Biol.* 217: 2531–2547. <https://doi.org/10.1083/jcb.201708096>
- Miller, D. M., I. Ortiz, G. C. Berliner, and H. F. Epstein, 1983 Differential localization of two myosins within nematode thick filaments. *Cell* 34: 477–490. [https://doi.org/10.1016/0092-8674\(83\)90381-1](https://doi.org/10.1016/0092-8674(83)90381-1)
- Noma, K., A. Goncharov, M. H. Ellisman, and Y. Jin, 2017 Microtubule-dependent ribosome localization in *C. elegans* neurons. *Elife* 6: e26376. <https://doi.org/10.7554/eLife.26376>
- Petrash, H. A., A. Philbrook, M. Haburcak, B. Barbagallo, and M. M. Francis, 2013 ACR-12 ionotropic acetylcholine receptor complexes regulate inhibitory motor neuron activity in *Caenorhabditis elegans*. *J. Neurosci.* 33: 5524–5532. <https://doi.org/10.1523/JNEUROSCI.4384-12.2013>
- Philbrook, A., S. Ramachandran, C. M. Lambert, D. Oliver, J. Florman *et al.*, 2018 Neurexin directs partner-specific synaptic connectivity in *C. elegans*. *Elife* 7: e35692. <https://doi.org/10.7554/eLife.35692>
- Praitis, V., E. Casey, D. Collar, and J. Austin, 2001 Creation of low-copy integrated transgenic lines in *Caenorhabditis elegans*. *Genetics* 157: 1217–1226.
- Remington, S. J., 2011 Green fluorescent protein: a perspective. *Protein Sci.* 20: 1509–1519. <https://doi.org/10.1002/pro.684>
- Schwartz, M. L., and E. M. Jorgensen, 2016 SapTrap, a toolkit for high-throughput CRISPR/Cas9 gene modification in *Caenorhabditis elegans*. *Genetics* 202: 1277–1288. <https://doi.org/10.1534/genetics.115.184275>
- Tanenbaum, M. E., L. A. Gilbert, L. S. Qi, J. S. Weissman, and R. D. Vale, 2014 A protein-tagging system for signal amplification in gene expression and fluorescence imaging. *Cell* 159: 635–646. <https://doi.org/10.1016/j.cell.2014.09.039>
- Terpe, K., 2003 Overview of tag protein fusions: from molecular and biochemical fundamentals to commercial systems. *Appl. Microbiol. Biotechnol.* 60: 523–533. <https://doi.org/10.1007/s00253-002-1158-6>
- Von Stetina, S. E., M. Treinin, and D. M. Miller, III, 2006 The motor circuit. *Int. Rev. Neurobiol.* 69: 125–167. [https://doi.org/10.1016/S0074-7742\(05\)69005-8](https://doi.org/10.1016/S0074-7742(05)69005-8)
- White, J. G., E. Southgate, J. N. Thomson, and S. Brenner, 1986 The structure of the nervous system of the nematode *Caenorhabditis elegans*. *Philos. Trans. R. Soc. Lond. B Biol. Sci.* 314: 1–340.

Communicating editor: O. Hobert